

# SnO<sub>2</sub>/reduced graphene oxide composite films for electrochemical applications



E.A. Bondarenko<sup>a</sup>, A.V. Mazanik<sup>a,\*</sup>, E.A. Streltsov<sup>a</sup>, A.I. Kulak<sup>b</sup>, O.V. Korolik<sup>a</sup>

<sup>a</sup> Belarusian State University, Nezalezhnastsi Av. 4, Minsk 220030, Belarus

<sup>b</sup> Institute of General and Inorganic Chemistry, National Academy of Sciences of Belarus, Surganova str., 9/1, Minsk 220072, Belarus

## ARTICLE INFO

### Article history:

Received 13 July 2015

Received in revised form

14 September 2015

Accepted 3 October 2015

### Keywords:

Tin oxide

Reduced graphene oxide (rGO)

Colloid

Composite

Thin film

Anodic oxidation

## ABSTRACT

SnO<sub>2</sub>/GO (GO is graphene oxide) composite films with GO mass fraction  $w_c$  ranging from 0.01 to 80% have been prepared using colloidal solutions. Heat treatment of SnO<sub>2</sub>/GO films in Ar atmosphere at 400 °C leads to GO reduction accompanied by partial exfoliation and decreasing of the particle thickness. SnO<sub>2</sub>/rGO (rGO is reduced GO) film electrodes demonstrate a high electrocatalytic activity in the anodic oxidation of inorganic (iodide-, chloride-, sulfite-anions) and organic (ascorbic acid) substances. The increase of the anodic current in these reactions is characterized by overpotential inherent to the individual rGO films and exchange current density grows linearly with rGO concentration at  $w_c \leq 10\%$  indicating that the rGO particles in composites act as sites of electrochemical process. The SnO<sub>2</sub>/rGO composite films, in which the chemically stable oxide matrix encapsulates the rGO inclusions, can be considered as a promising material for applied electrochemistry.

© 2015 Elsevier B.V. All rights reserved.

## 1. Introduction

Tin dioxide SnO<sub>2</sub> belongs to wide band-gap oxide semiconductors (band gap energy  $E_g = 3.54$  eV) with *n*-type conductivity [1,2]. The tuning of SnO<sub>2</sub> resistivity is achieved by its doping with fluorine, antimony and other elements (Al, Ga, Cr, Zn, Pt, etc.) [3–7]. Highly doped degenerate SnO<sub>2</sub> films especially in combination with indium oxide (indium tin oxide – ITO) are widely used as a conductive material transparent in the visible spectral region [3,4]. High electrical conductivity and corrosion resistance, large anodic overpotential of oxygen evolution from water, as well as a low cost promote the application of SnO<sub>2</sub> as thin film electrodes for oxidizing and destroying of organic pollutants in waste water [8–10].

Composite film electrodes formed on the titanium substrate and based on SnO<sub>2</sub> and such oxides as RuO<sub>2</sub>, IrO<sub>2</sub>, Co<sub>3</sub>O<sub>4</sub> are of a great interest for the chloric electrolysis [11,12]. In such anodes, oxides of the platinum-group metals or the cobalt oxide serve mainly as the electrocatalytic conductive additives, whereas the tin oxide acts as a stabilizing matrix.

Along with the above-listed oxides (RuO<sub>2</sub>, IrO<sub>2</sub>, Co<sub>3</sub>O<sub>4</sub>), highly-conductive forms of carbon (carbon nanotubes, graphene, reduced graphene oxide) can be used to increase the electrical conductivity of such composite electrodes. Reduction of graphene oxide is necessary to enhance its electrical conductivity, because some of carbon atoms in GO have chemical bonds with oxygen in different functional groups (hydroxyl, carbonyl, carboxyl, ether, etc.) leading to a drastic decrease in electrical conductivity due to a damage of the delocalized  $\pi$ -bonds system. GO reduction can be performed using reducing agents (for example, N<sub>2</sub>H<sub>4</sub>, NaBH<sub>4</sub>), UV-radiation, ultrasound, etc. [13,14]. In the synthesis of composites with SnO<sub>2</sub>, Sn(II) atoms can act as a reductant [15]. SnO<sub>2</sub>/graphene and SnO<sub>2</sub>/rGO heterostructures are the promising materials for application as anode in lithium ion batteries [16–20], counter electrode in dye-sensitized solar cells [21], photocatalysts for organic oxidation [22], gas sensors [23].

One of the main methods to form SnO<sub>2</sub> films is a high-temperature oxidative pyrolysis of tin compounds (most often, SnCl<sub>4</sub>) on the surface of substrates heated up to high temperatures (~500 °C) [8]. However, such approach does not allow obtaining SnO<sub>2</sub> based composites doped with thermally unstable compounds prone to oxidation, e.g. highly-dispersive carbon. Therefore, low-temperature techniques should be applied for the preparation of SnO<sub>2</sub>/rGO composites, for instance, co-deposition from solutions, where graphene-oxide colloids are used as a carbon precursor [24].

\* Corresponding author. Tel.: +375 292769624; fax: +375 172095445.

E-mail addresses: [mazanikalexander@gmail.com](mailto:mazanikalexander@gmail.com) (A.V. Mazanik), [kulak@gic.bas-net.by](mailto:kulak@gic.bas-net.by) (A.I. Kulak).

The literature analysis shows that the SnO<sub>2</sub>/rGO film heterostructures still have not been considered as electrode for anodic oxidation processes. Thus, the aim of this study is to investigate the electrocatalytic properties of the composite electrodes based on SnO<sub>2</sub> and reduced graphene oxide in reactions of anodic oxidation of inorganic (chloride- and iodide-anions, SO<sub>3</sub><sup>2-</sup>) and organic (ascorbic acid) substances. The SnO<sub>2</sub>/rGO films with a wide range of highly-dispersive carbon phase concentration (mass fraction varies from 0.01% to 80%) have been prepared from the colloidal co-solutions of tin oxide and graphene-oxide. Phase composition, microstructure, defectiveness, as well as electrical and optical properties of the SnO<sub>2</sub>/rGO composite films have been characterized by a complex of experimental techniques. The influence of the carbon phase concentration on the anodic reactions was studied in terms of overpotential and exchange current densities.

## 2. Experimental

SnO<sub>2</sub> colloidal solution was prepared by adding a precooled NH<sub>3</sub> solution (*w* = 12.5%) to SnCl<sub>4</sub> dissolved in water at 0 °C to attain pH 11. The prepared gel was centrifuged, the precipitate was separated, washed with water and dialysed for 2 days. The SnO<sub>2</sub> content in the obtained colloidal solution determined by the gravimetric method was 70 mg/ml.

The methods described in [25,26] were used for the preparation of GO aqueous colloidal solution; a stable dark brown GO sol (pH ~6) containing 9 mg/ml was obtained.

The SnO<sub>2</sub>/GO films with a mass fraction of the carbon phase *w<sub>C</sub>* varied in the range from 0.01% to 80% were formed by spin coating of colloidal co-solutions with different mass fraction of SnO<sub>2</sub> and GO on the fluorine doped tin oxide (FTO) or glass substrates. The individual SnO<sub>2</sub> and GO films were also synthesized for reference experiments. The film thickness according to SEM was a few hundreds of nanometers. The composites were annealed for 1 h at 400 °C in Ar atmosphere for GO reduction. It should be noted that “GO” and “rGO” terms below correspond to carbon phase in the studied composites before and after annealing, respectively, and the mass fraction of the carbon phase refers to the as-deposited films and does not take into account the mass losses under annealing.

X-ray diffraction analysis was carried out with a Rigaku ULTIMA IV diffractometer (Bragg–Brentano geometry, Cu K $\alpha$  emission, 0.5 deg./min). Scanning electron microscopy (SEM) in both the secondary electron (SE) and backscattered electron (BSE) modes was performed using Hitachi S 4800 (field emission cathode) and LEO 1455 VP microscopes with an energy dispersive X-ray (EDX) analyzer. Atomic force microscopy (AFM) was performed with a Solver P47-PRO microscope in the tapping mode. Transmission spectra were taken with a MC122 spectrometer (Proscan Special Instruments, Belarus). Raman spectra were measured using a Nanofinder HE confocal spectrometer (Lotis TII, Belarus–Japan) with a 532 nm solid-state laser as an excitation source. Incident optical power was attenuated to a few tens of microwatts to minimize a thermal impact. Back-scattered light without analysis of its polarization was dispersed with a spectral resolution of 2.5 cm<sup>-1</sup> and detected with a cooled CCD-matrix. Signal acquisition time was equal to 120 s. The excitation spot diameter was about 1  $\mu$ m. Spectral calibration was done using a built-in gas-discharge lamp providing accuracy better than 2.5 cm<sup>-1</sup>.

Thermogravimetric (TG) analyses were performed in argon atmosphere at a scanning rate of 5 °C/min with a NETZSCH STA 409 PC/PG (Germany) DTA/TGA analyzer in the temperature range of 25–800 °C.

Electrochemical measurements were performed with a P-8 potentiostat (Elins, Russia) in a standard 50 ml three-electrode cell

with a Pt counter-electrode and an Ag|AgCl|KCl (sat.) electrode as a reference one (+0.201 V vs standard hydrogen electrode). All potentials are given relative to this reference electrode. In photoelectrochemical experiments, 1 M Na<sub>2</sub>SO<sub>3</sub> solution was used as electrolyte, as the sulphite-anions are effective photohole acceptors preventing a possible rGO photooxidation. A mercury-xenon UV lamp (30 mW/cm<sup>2</sup>, spectral range from 220 to 350 nm) was used as a light source.

## 3. Results and discussion

### 3.1. Characterization of SnO<sub>2</sub> and SnO<sub>2</sub>/GO films

The SnO<sub>2</sub> films deposited from colloidal solutions are characterized by a uniform surface and contain no pronounced microheterogeneities both before and after heat treatment (Fig. 1a). SEM (the SE mode, Fig. 1) and AFM (Fig. S1a and b) studies reveal no pronounced changes in the surface morphology at low concentrations of the carbon phase in the films (*w<sub>C</sub>* ≤ 10%) indicating only a slight increase of the surface roughness and phase shift dispersion in AFM images (Fig. S1c and d). At the same time, the irregularly-shaped inclusions are clearly visible in the SEM images (the BSE mode) for GO doped films (Fig. S2). According to the EDX and micro-Raman analyses, these inclusions represent the particles of carbon phase, which formation is likely to be due to the coagulation of GO particles when GO and SnO<sub>2</sub> solutions are mixing. Heat treatment of the SnO<sub>2</sub>/GO films reduces a contrast in the BSE mode (Fig. S2) indicating a decrease in the thickness of carbon inclusions which correlates with the XRD results presented below.

Transmission spectra of the films before and after annealing are given in Fig. 2. As it is seen, the annealing leads to some decrease in transmission; however it exceeds 85% over the whole spectral range. The qualitatively similar influence of graphene oxide reduction on the optical transmission was noticed in Ref. [27].

The TG and respective differential thermogravimetric (DTG) curves of the GO presented in Fig. 3 showed a characteristic decomposition process with an onset temperature at 29.9 mass% loss of 165 °C and the temperature at maximum mass loss rate of 214 °C. The abrupt mass lost is related to an exothermic (*t<sub>max</sub>* = 216 °C, 752 J/g) decomposition of oxygen-containing groups. This process is accompanied by the release of CO<sub>2</sub> and may lead to exfoliation of GO [28]. Significant mass loss at high temperatures ranging from 465 to 665 °C is associated with a gradual destruction of GO. An initial 15.2 mass% loss at temperatures ranging from 25 to 140 °C is attributed with adsorbed water removing.

The TGA/DTG curves describing the thermal processes in SnO<sub>2</sub> contain the regions of mass loss related to water removing (endothermic effect, *t<sub>max</sub>* = 100 °C); in the range from 25 to 300 °C the total mass loss equals to 12.3%. An exothermic effect presumably related to the phase transition in oxide is seen on the DTA curve at 513 °C.

Thermal processes in the 20% GO + 80% SnO<sub>2</sub> composite can be considered in the first approximation as a superposition of the above-discussed processes in GO and SnO<sub>2</sub>. There is a peak corresponding to destruction of the oxygen-containing groups in the range from 165 to 235 °C, although its maximum is shifted to slightly lower temperatures (*t<sub>max</sub>* = 199 °C). A gradual mass loss from 300 to 600 °C equals to 11.8% being somewhat different from the literature data, according to which the weight decreases more abruptly at temperatures above 400 °C and until 650 °C [16,29]. This difference could be explained by more tight contact between GO and SnO<sub>2</sub> in our composites that determines catalytic or reducing impact of SnO<sub>2</sub> on the thermodestruction of graphene-oxide. In the range of linear mass change with temperature from 500 to 600 °C the mass loss of the composite equals to 7.8%, whereas the mass

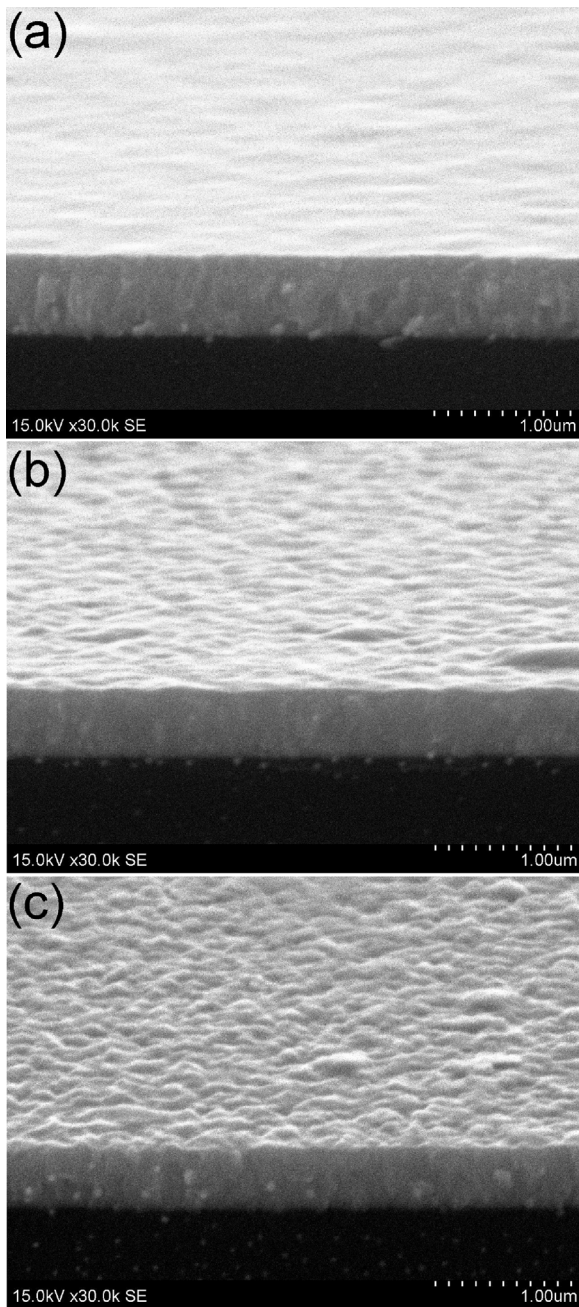


**Fig. 1.** SEM images (SE mode) of the films: (a) individual  $\text{SnO}_2$ ; (b, c)  $\text{SnO}_2/\text{rGO}$  with mass fraction of carbon phase  $w_c = 1\%$  and  $w_c = 10\%$ , respectively.

losses of the individual graphene-oxide and  $\text{SnO}_2$  at the same temperature range are equal to 28% and 0.4%, respectively. Such mass loss of the composite corresponds with an adequate accuracy to the loss determined by the destruction of graphene-oxide being its part.

The X-ray diffraction patterns of both the as-deposited and annealed films reveal in the studied range  $5^\circ \leq 2\theta \leq 60^\circ$  only one reflex corresponding to diffraction on the (002) plane family of graphite-like carbon (Fig. 4). Position of the (002) reflex points out to effective graphite exfoliation when preparing GO and is in agreement with results observed for graphene oxide in many works [14,27,30,31]. Annealing leads to its significant weakening, a slight shift to the smaller angle range and remarkable broadening (Table 1). Broadening of XRD reflex can be determined by the decrease in coherent-scattering region (CSR) size, as well as by

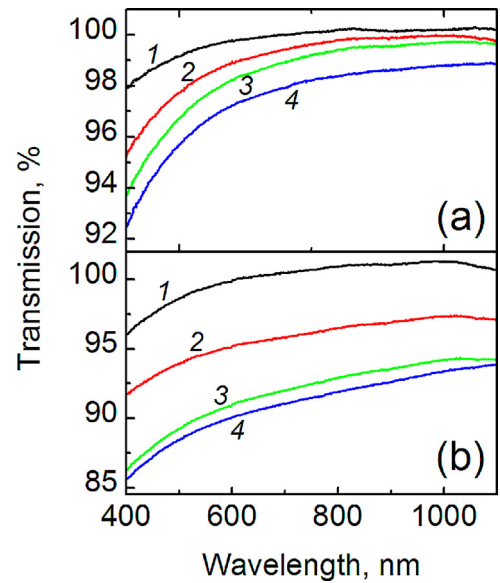


**Fig. 2.** Transmission spectra of the composite films before (a) and after (b) annealing at  $400^\circ\text{C}$  for 1 h in Ar. Mass fraction of the carbon phase in the film is 0% (1), 20% (2), 40% (3), and 100% (4).

transformation of carbon phase into amorphous state. However, amorphization is not supported by results of the Raman spectroscopy (see below). Table 1 contains also the interplanar distance and CSR size values estimated according to the Bragg and Sherer equations, respectively. The presented data point out to the

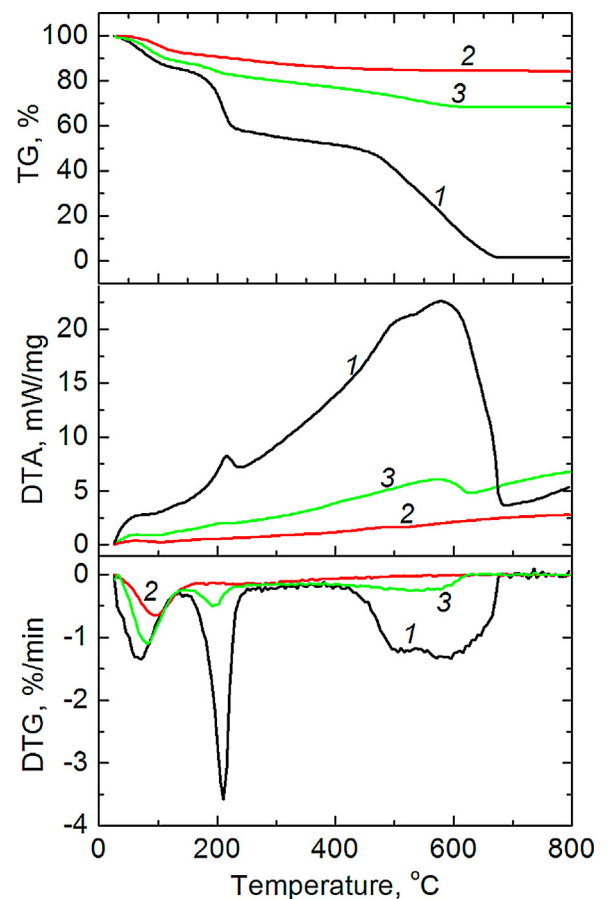


**Fig. 3.** TG, differential thermal analysis (DTA), and DTG curves for GO (1),  $\text{SnO}_2$  (2), and 20% GO + 80%  $\text{SnO}_2$  (3) films.

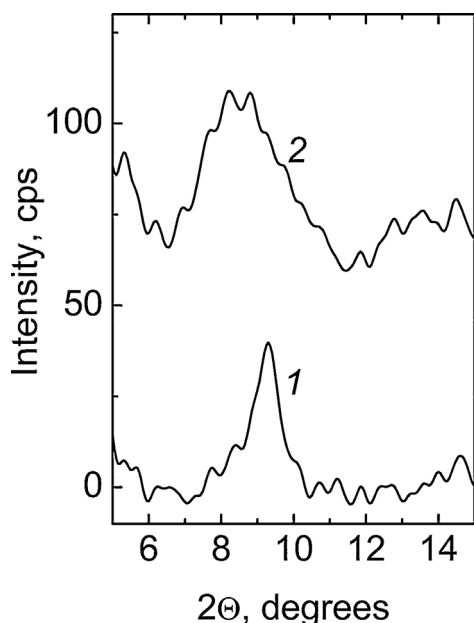


**Fig. 4.** X-ray diffraction patterns of composite film at  $w_C = 7\%$  before (1) and after (2) annealing at  $400\text{ }^\circ\text{C}$ . The curves are arranged along the Y-axis for convenience.

annealing-induced exfoliation of graphene oxide that results in increase of the interplanar distance, as well as 4–6-fold decrease in the number of carbon layers in the particles. Similar transformations of XRD patterns have been observed in [14] during photochemical reduction of graphene oxide.

Raman spectroscopy is known to be very informative technique to characterize different carbon materials. As is known [32–35], the most intensive bands in Raman spectra of  $sp^2$  carbon networks are so-called G band (doubly degenerate phonon mode at the Brillouin zone center), D band (disorder-induced phonon mode corresponding to scattering on the K-point phonon), and 2D band (overtone of the D band).

Typical Raman spectra of the composite films before and after annealing are presented in Fig. 5. In the spectra of both the as-deposited and annealed films one can see the D and G bands, as well as three bands in the range of Raman shifts above  $2500\text{ cm}^{-1}$ : 2D band, D+G band, and a band (denoted as HF), which position allows us ascribing it to the overtone of G band [36] or to OH group stretching vibration [37]. The experiments have demonstrated a good reproducibility of spectra shape under excitation of different points on the surface indicating an identity of carbon phase properties over the whole film. In the Raman spectra of both the as-deposited and annealed films there are no bands inherent to  $\text{SnO}_2$  which is in agreement with its X-ray amorphism.

Fitting of Raman spectra by superposition of the Lorentz lines enabled one to determine position, spectral width (FWHM) and area (frequency integrated intensity) of the observed bands. These results are summarized in Table S1. As it is seen from Fig. 5 and Table S1, annealing of the films modifies their Raman spectra leading to (i) a signal weakening; (ii) a slight (by  $2\text{--}5\text{ cm}^{-1}$ ) shift of the G band to the region of larger wavenumbers; (iii) a remarkable increase in the D band width, whereas the G band width practically does not change; (iv) 1.3–1.4-fold increase of the D and G bands

area ratio. All these regularities point out to an increase in the GO defectiveness as the functional groups leave the material during its reduction which is in agreement with results of other researches [38–42], where similar changes in Raman spectra were observed. In particular, intensity decrease in Raman spectra upon annealing can be attributed to disordering of crystalline structure, because the signal intensity in Raman spectra is known to increase with material crystallinity. At the same time, Raman spectra shape for the annealed films is significantly different from Raman spectrum of amorphous carbon (see, for example, Ref. [43]) indicating conservation of crystalline structure of carbon phase. The observed G band shift may be related to an increase in  $D^*$  band ( $\sim 1620\text{ cm}^{-1}$ ) intensity and impossibility to resolve the G and  $D^*$  bands due to their large spectral width [44]. Increase in the D band width with preservation of the G band width after annealing means that scattering of the short-wavelength phonons responsible for the D band increases sharply, whereas the efficiency of scattering of the long-wavelength phonons corresponding to the G band remains constant after annealing. Therefore, the observed increase of  $A_D/A_G$  values indicates first of all an increase of point defect concentration due to removal of the functional groups during annealing. The intensity ratio of the 2D and G bands which is known as a parameter to distinguish graphite and graphene [45], changes insignificantly after annealing. It is in agreement with results of other researches [39], where a remarkable transformation of GO Raman spectra with attainment of the shape characteristic for graphene is observed only at much higher reduction temperature as compared to that in our experiments.

As it is seen from Table S1, the spectral parameters of the D and G bands are practically independent of GO content in the composite films. The exception is the D band width and D to G bands area ratio  $A_D/A_G$ , which tend to an increase with the GO concentration. As it is demonstrated above by the XRD analysis, the film annealing leads to the exfoliation of the carbon particles. Such process will promote an increase in their defectiveness in the case of tight packing in the film. One can presume that in the  $\text{SnO}_2/\text{GO}$  composites the  $\text{SnO}_2$  matrix acts as a damper reducing a damage of the carbon particles during annealing.

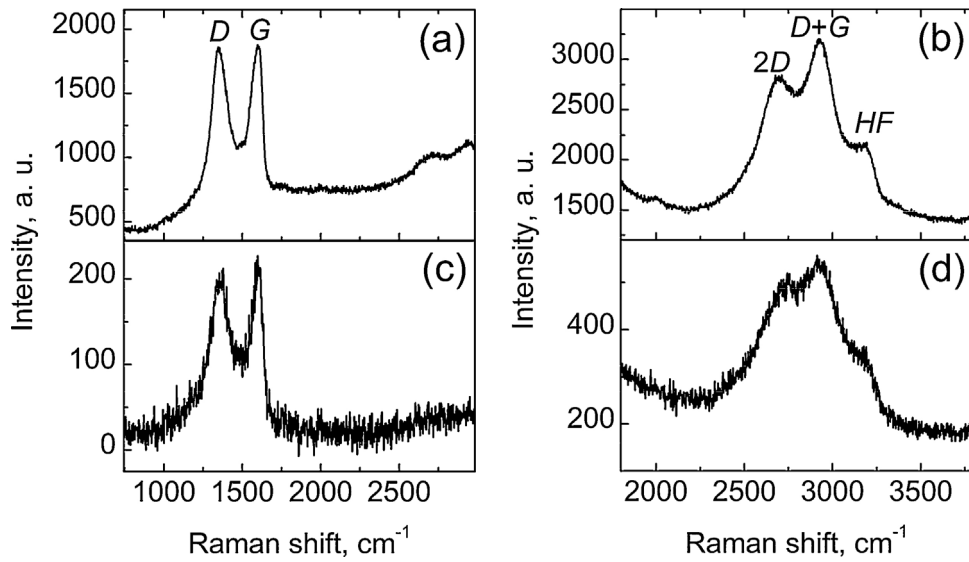
### 3.2. Photoelectrochemical and electrocatalytic properties

$\text{SnO}_2$  electrodes demonstrate electrochemical behavior typical for n-type semiconductors locking the anodic current in aqueous solutions of indifferent electrolytes ( $\text{Na}_2\text{SO}_3$ ,  $\text{Na}_2\text{SO}_4$ ,  $\text{NaClO}_4$ ) in the relatively wide electrode potential range (Fig. 6, curve 1). At the same time, the Faraday processes are possible when the  $\text{SnO}_2$  electrodes are illuminated by photons with the energy exceeding the band gap (Fig. 6, curve 2). Photocurrent onset-potential (in the first approximation equal to the flat-band potential of semiconductor) corresponds to  $-0.2\text{ V}$ .

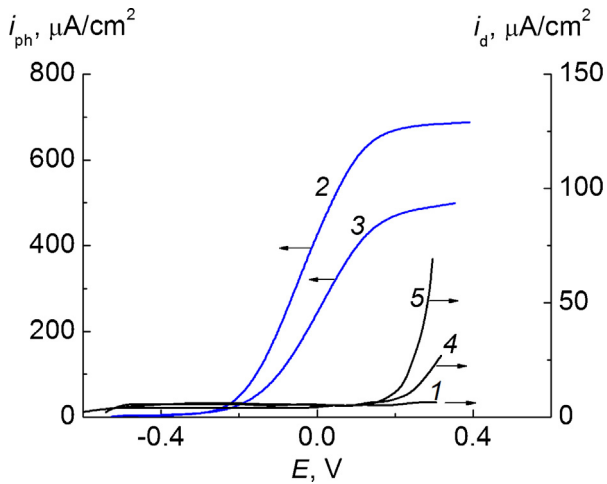
Addition of rGO into the  $\text{SnO}_2$  film leads to a remarkable (approximately in 1.5 times) decrease in the anodic photocurrent density  $i_{ph}$  even at  $w_C = 1\%$  (Fig. 6, curves 2 and 3). A further  $i_{ph}$  reduction is observed with the increase of the carbon phase concentration in the films (Fig. 7, curve 1) and the  $\text{SnO}_2/\text{rGO}$  electrodes lose their photoelectrochemical activity almost completely at  $w_C \geq 20\%$ . A drop in photoelectrochemical activity can be caused by (i) redistribution of the electrode potential from semiconductor oxide to graphene nanophase, as well as by (ii) increase in

**Table 1**  
Results of XRD characterization of carbon phase in composite films.

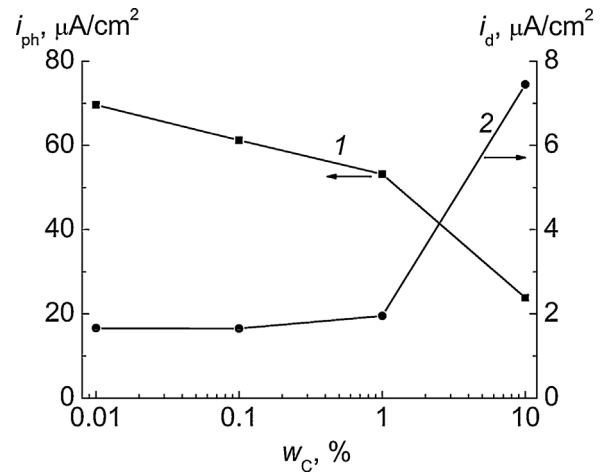
State of film	Peak position $2\theta$ ( $^\circ$ )	Peak FWHM ( $^\circ$ )	Interplanar spacing $d_{002}$ (nm)	CSR (thickness) (nm)	Number of carbon layers
Before annealing	9.2	0.7	0.95	12	12–13
After annealing	8.6	3.3	1.0	2.5	2–3



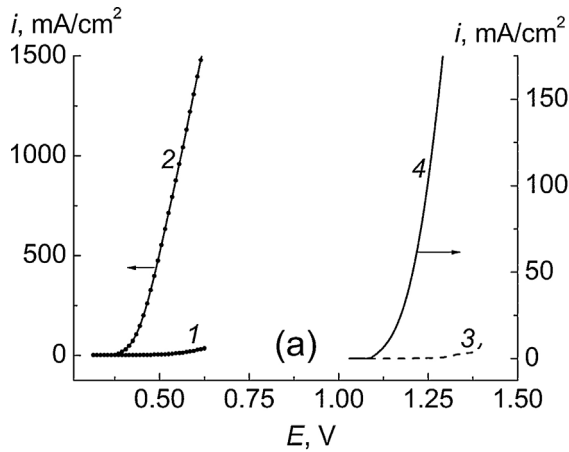
**Fig. 5.** Raman spectra of SnO<sub>2</sub>/GO film at  $w_C = 10\%$  before (a, b) and after (c, d) annealing at 400 °C. High-frequency region spectra (b, d) were obtained at one order higher excitation power.



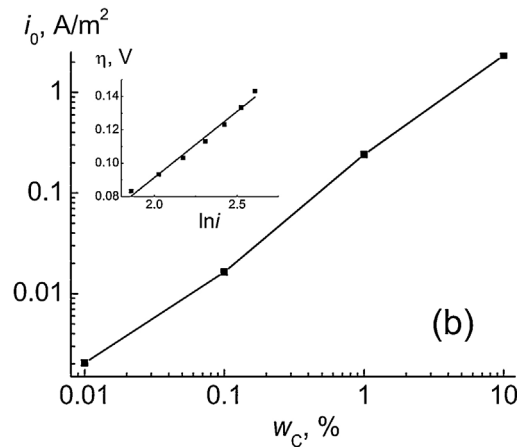
**Fig. 6.** Potentiodynamic polarization curves for SnO<sub>2</sub> (1, 2), SnO<sub>2</sub>/rGO (3, 4) and rGO (5). Mass fraction of the carbon phase in the film  $w_C = 1\%$ . Electrolyte: 0.5 M Na<sub>2</sub>SO<sub>3</sub>.  $dE/dt = 20$  mV/s.



**Fig. 7.** Photocurrent (1) and dark anodic current (2) for the SnO<sub>2</sub>/rGO electrodes depending on the mass fraction of carbon phase in the film. Electrode potential  $E = 0.15$  V. Electrolyte: 0.5 M Na<sub>2</sub>SO<sub>3</sub>.



**Fig. 8.** (a) Anodic polarization curves for SnO<sub>2</sub> (1, 3) and SnO<sub>2</sub>/rGO ( $w_C = 20\%$ ) electrodes (2, 4) in the 0.5 M Na<sub>2</sub>SO<sub>4</sub> + 0.05 M KI + 0.001 M I<sub>2</sub> (1, 2) and 4 M NaCl acidified by HCl (pH 2, 3, 4) solutions. Curves 1, 2 are taken under the steady-state conditions, curves 3, 4 – with potential sweep rate of 1 mV/s. (b) Exchange current density in 0.5 M Na<sub>2</sub>SO<sub>4</sub> + 0.05 M KI + 0.001 M I<sub>2</sub> solution vs carbon phase mass fraction. Inset: Tafel plot for SnO<sub>2</sub>/rGO ( $w_C = 10\%$ ) electrode.



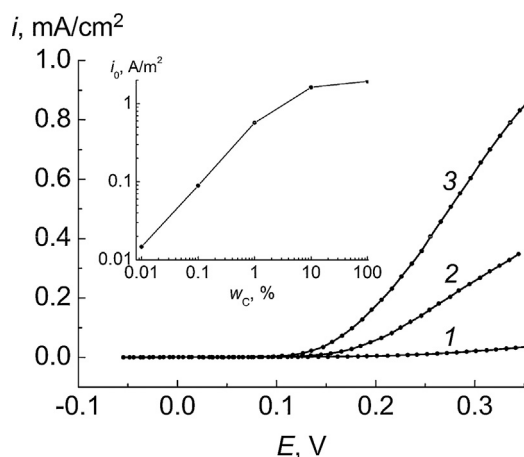


**Fig. 9.** Stationary anodic polarization curves for the SnO<sub>2</sub>/rGO electrodes in 0.5 M Na<sub>2</sub>SO<sub>4</sub> + 0.02 M ascorbic acid solution. Mass fraction of the carbon phase in the films (%): 1–0; 2–1; 3–10. Inset: exchange current density vs mass fraction of the carbon phase.

recombination of photocarriers generated in SnO<sub>2</sub>. Simultaneously, the dark anodic current at  $E > +0.2$  V related to oxidation of the sulphite-anions appears when the carbon phase is added into the film (Fig. 6, curve 4). This current increases with the carbon phase concentration increase (Fig. 7, curve 2). Note that the anodic processes on the surface of individual rGO and composite films occur at the same potential values (Fig. 6, curves 4 and 5).

High electrocatalytic activity of the SnO<sub>2</sub>/rGO electrodes manifests itself also in reactions of anodic oxidation of the iodide and chloride anions (Fig. 8), which flow with a small overpotential ( $\eta \sim 10$ –20 mV). The polarization curves are linearized at their initial parts in the Tafel coordinates ( $\ln i - \eta$ ) indicating that the overpotential is electrochemical. Fig. 8b demonstrates that in the range  $w_C = 0.01$ –10% the exchange current density  $i_0$  growth approximately linearly with increase of the carbon mass fraction.

Anodic oxidation of the ascorbic acid was investigated as a test reaction of oxidation of organic substances (Fig. 9). The anodic process occurs at  $E > +100$  mV and is characterized by a sharp rise in the current with increase of  $w_C$  value. Dependence of the exchange current density on the carbon phase mass fraction  $w_C$  (inset in Fig. 9) enables one to conclude that the most remarkable  $i_0$  growth takes place in the range  $w_C = 0.01$ –10% (i.e., approximately in the same concentration range as for the above-considered process of the iodide-anion oxidation). The exchange current density for the individual rGO film presented at the same plot has the maximal value indicating that the electrochemical process is localized on the surface of the rGO inclusions.

#### 4. Conclusions

The SnO<sub>2</sub>/GO composite films with the GO mass fraction varied in a wide range (0.01–80%) have been synthesized using GO in SnO<sub>2</sub> colloidal solutions. According to the TGA, Raman spectroscopy, and XRD analyses, annealing of the films in argon at 400 °C reduces the graphene oxide which is accompanied by introduction of point defects into carbon particles, as well as their partial exfoliation and reduction of thickness down to 2–3 carbon layers.

The SnO<sub>2</sub>/rGO film electrodes demonstrate a high electrocatalytic activity in dark processes of anodic oxidation of both inorganic (I<sup>-</sup>, Cl<sup>-</sup>, SO<sub>3</sub><sup>2-</sup>-anions) and organic (ascorbic acid) substances. The anodic current grows with an overpotential inherent to the individual rGO, and exchange current density increases linearly

with the increase of the carbon phase concentration at  $w_C \leq 10\%$  indicating the fact that the rGO inclusions act as sites of the anodic process localization.

The obtained results demonstrate that the SnO<sub>2</sub>/rGO composite films combining a high chemical stability of the oxide matrix encapsulating the rGO inclusions and a high electrical conductivity and electrocatalytic activity are promising for various applications in electrochemistry (electrochemical synthesis, waste water treatment, etc.).

#### Acknowledgements

The work was financially supported by the Research Programs “Electronics and Photonics” (contract No 2.2.19) and “Chemical Technologies and Materials, Natural and Resource Potential” (contract No 1.39) of the Republic of Belarus. We thank Dr. S.V. Gusakova, Dr. L.V. Baran, and Dr. S.V. Zlotski for carrying out the SEM/EDX, AFM, and XRD experiments, respectively.

#### Appendix A. Supplementary data

Supplementary data associated with this article can be found, in the online version, at <http://dx.doi.org/10.1016/j.mseb.2015.10.002>.

#### References

- [1] Z.M. Jarzelski, J.P. Marton, J. Electrochem. Soc. 123 (1976) 199C–205C, <http://dx.doi.org/10.1149/1.2133010>.
- [2] Z.M. Jarzelski, J.P. Marton, J. Electrochem. Soc. 123 (1976) 333C–346C, <http://dx.doi.org/10.1149/1.2132647>.
- [3] K.L. Chopra, S. Major, D.K. Pandya, Thin Solid Films 102 (1983) 1–46, [http://dx.doi.org/10.1016/0040-6090\(83\)90256-0](http://dx.doi.org/10.1016/0040-6090(83)90256-0).
- [4] G.J. Exarhos, X.-D. Zhou, Thin Solid Films 515 (2007) 7025–7052, <http://dx.doi.org/10.1016/j.tsf.2007.03.014>.
- [5] Z.M. Jarzelski, Phys. Status Solidi A 71 (1982) 13–41, <http://dx.doi.org/10.1002/pssa.2210710102>.
- [6] F. Vicent, E. Morallon, C. Quijada, J.L. Vazquez, A. Aldaz, F. Cases, J. Appl. Electrochem. 28 (1998) 607–612, <http://dx.doi.org/10.1023/A:1003250118996>.
- [7] Z.M. Jarzelski, J.P. Marton, J. Electrochem. Soc. 123 (1976) 299C–310C, <http://dx.doi.org/10.1149/1.2133090>.
- [8] R. Kotz, S. Stucki, B. Carcer, J. Appl. Electrochem. 21 (1991) 14–20, <http://dx.doi.org/10.1007/BF01103823>.
- [9] S. Stucki, R. Kotz, B. Carcer, W. Suter, J. Appl. Electrochem. 21 (1991) 99–104, <http://dx.doi.org/10.1007/BF01464288>.
- [10] C. Comninellis, A. Nerini, J. Appl. Electrochem. 25 (1995) 23–28, <http://dx.doi.org/10.1007/BF00251260>.
- [11] L. Nanni, S. Polizzi, A. Benedetti, A. De Battisti, J. Electrochem. Soc. 146 (1999) 220–225, <http://dx.doi.org/10.1149/1.1391590>.
- [12] A.I. Onuchukwu, S. Trasatti, J. Appl. Electrochem. 21 (1991) 858–862, <http://dx.doi.org/10.1007/BF01042451>.
- [13] J.K. Wassei, R.B. Kaner, Acc. Chem. Res. 46 (2013) 2244–2253, <http://dx.doi.org/10.1021/ar300184v>.
- [14] A.L. Stroyuk, N.S. Andryushina, N.D. Shcherban, V.G. Il'in, V.S. Efanov, I.B. Yanchuk, S.Y. Kuchmii, V.D. Pokhodenko, Theor. Exp. Chem. 48 (2012) 2–13, <http://dx.doi.org/10.1007/s11237-012-9235-0>.
- [15] B. Lee, S.C. Han, M. Oh, M. Soo Lah, K.-S. Sohn, M. Pyo, Electrochim. Acta 113 (2013) 149–155, <http://dx.doi.org/10.1016/j.electacta.2013.09.093>.
- [16] J. Liang, W. Wei, D. Zhong, Q. Yang, L. Li, L. Guo, ACS Appl. Mater. Interfaces 4 (2012) 454–459, <http://dx.doi.org/10.1021/am201541s>.
- [17] P. Lian, X. Zhu, S. Liang, Z. Li, W. Yang, H. Wang, Electrochim. Acta 56 (2011) 4532–4539, <http://dx.doi.org/10.1016/j.electacta.2011.01.126>.
- [18] H. Song, N. Li, H. Cui, C. Wang, J. Mater. Chem. A 1 (2013) 7558–7562, <http://dx.doi.org/10.1039/C3TA11442B>.
- [19] B. Chen, H. Qian, J. Xu, L. Qin, Q.-H. Wu, Mi. Zheng, Q. Dong, J. Mater. Chem. A 2 (2014) 9345–9352, <http://dx.doi.org/10.1039/c4ta01493f>.
- [20] J. Lin, Z. Peng, C. Xiang, G. Ruan, Z. Yan, D. Natelson, J.M. Tour, ACS Nano 7 (2013) 6001–6006, <http://dx.doi.org/10.1021/nn4016899>.
- [21] F. Du, B. Yang, X. Zuo, G. Li, Mater. Lett. 158 (2015) 424–427, <http://dx.doi.org/10.1016/j.matlet.2015.06.012>.
- [22] J. Zhang, Z. Xiong, X.S. Zhao, J. Mater. Chem. 21 (2011) 3634–3640, <http://dx.doi.org/10.1039/C0JM03827J>.
- [23] Y. Chang, Y. Yao, B. Wang, H. Luo, T. Li, L. Zhi, J. Mater. Sci. Technol. 29 (2013) 157–160, <http://dx.doi.org/10.1016/j.jmst.2012.11.007>.
- [24] Z. Du, X. Yin, M. Zhang, Q. Hao, Y. Wang, T. Wang, Mater. Lett. 64 (2010) 2076–2079, <http://dx.doi.org/10.1016/j.matlet.2010.06.039>.

- [25] H. Bai, Y. Xu, L. Zhao, C. Li, G. Shi, Chem. Commun. (2009) 1667–1669, <http://dx.doi.org/10.1039/B821805F>.
- [26] H.A. Becceril, J. Mao, Z. Liu, R.M. Stoltenberg, Z. Bao, Y. Chen, ACS Nano 2 (2008) 463–470, <http://dx.doi.org/10.1021/nn700375n>.
- [27] N.S. Andryushina, O.L. Stroyuk, Appl. Catal. B: Environ. 148–149 (2014) 543–549, <http://dx.doi.org/10.1016/j.apcatb.2013.11.044>.
- [28] H.C. Schniepp, J.-L. Li, M.J. McAllister, H. Sai, M. Herrera-Alonso, D.H. Adamson, R.K. Prud'homme, R. Car, D.A. Saville, I.A. Aksay, J. Phys. Chem. B 110 (2006) 8535–8539, <http://dx.doi.org/10.1021/jp060936f>.
- [29] G. Neri, S.G. Leonardi, M. Latino, N. Donato, S. Baek, D.E. Conte, P.A. Russo, N. Pinna, Sens. Actuators B: Chem. 179 (2013) 61–68, <http://dx.doi.org/10.1016/j.snb.2012.10.031>.
- [30] L. Zhou, X. Yang, B. Yang, X. Zuo, G. Li, A. Feng, H. Tang, H. Zhang, M. Wu, Y. Ma, S. Jin, Z. Sun, X. Chen, J. Power Sources 272 (2014) 639–646, <http://dx.doi.org/10.1016/j.jpowsour.2014.06.172>.
- [31] I.K. Moon, J. Lee, R.S. Ruoff, H. Lee, Nat. Commun. 1 (2010), <http://dx.doi.org/10.1038/ncomms1067>, AN Article number 73, 6 pp.
- [32] F. Tuinstra, J.L. Koenig, J. Phys. Chem. 53 (1970) 1126–1130, <http://dx.doi.org/10.1063/1.1674108>.
- [33] A.C. Ferrari, J. Robertson, Phys. Rev. B 64 (2001) 075414, <http://dx.doi.org/10.1103/PhysRevB.64.075414>, 13 pp.
- [34] M.S. Dresselhaus, G. Dresselhaus, R. Saito, A. Jorio, Phys. Rep. 409 (2005) 47–99, <http://dx.doi.org/10.1016/j.physrep.2004.10.006>.
- [35] M.A. Pimenta, G. Dresselhaus, M.S. Dresselhaus, L.G. Cançado, A. Jorio, R. Saito, Phys. Chem. Chem. Phys. 9 (2007) 1276–1291, <http://dx.doi.org/10.1039/B613962K>.
- [36] G. Compagnini, P. Russo, F. Tomarchio, O. Puglisi, L. D'Urso, S. Scalese, Nanotechnology 23 (2012) 505601, <http://dx.doi.org/10.1088/0957-4484/23/50/505601>, 6 pp.
- [37] R. Hawaldar, P. Merino, M.R. Correia, I. Bdikin, J. Grácio, J. Méndez, J.A. Martín-Gago, M.K. Singh, Sci. Rep. 2 (2012) 682, <http://dx.doi.org/10.1038/srep00682>, 9 pp.
- [38] A. Abulizi, G.-H. Yang, J.-J. Zhu, Ultrason. Sonochem. 21 (2014) 129–135, <http://dx.doi.org/10.1016/j.ultsonch.2013.07.013>.
- [39] J. Lim, K. Choi, J.R. Rani, J.-S. Kim, C. Lee, J.H. Kim, S.C. Jun, J. Appl. Phys. 113 (2013) 183502, <http://dx.doi.org/10.1063/1.4803713>, 5 pp.
- [40] H.F. Teoh, Y. Tao, E.S. Tok, G.W. Ho, C.H. Sow, Appl. Phys. Lett. 98 (2011) 173105, <http://dx.doi.org/10.1063/1.3580762>, 3 pp.
- [41] A. Kumar, A.L.M. Reddy, A. Mukherjee, M. Dubey, X. Zhan, N. Singh, L. Ci, W.E. Billups, J. Nagurny, G. Mital, P.M. Ajayan, ACS Nano 5 (2011) 4345–4349, <http://dx.doi.org/10.1021/nn201527p>.
- [42] C. Chen, M. Long, M. Xia, C. Zhang, W. Cai, Nanoscale Res. Lett. 7 (2012) 101, <http://dx.doi.org/10.1186/1556-276X-7-101>, 5 pp.
- [43] A.C. Ferrari, J. Robertson, Philos. Trans. R. Soc. Lond. A 362 (2004) 2477–2512, <http://dx.doi.org/10.1098/rsta.2004.1452>.
- [44] L.G. Cançado, A. Jorio, E.H. Martins Ferreira, F. Stavale, C.A. Achete, R.B. Capaz, M.V.O. Moutinho, A. Lombardo, T.S. Kulmala, A.C. Ferrari, Nano Lett. 11 (2011) 3190–3196, <http://dx.doi.org/10.1021/nl201432g>.
- [45] A.C. Ferrari, J.C. Meyer, V. Scardaci, C. Casiraghi, M. Lazzeri, F. Mauri, S. Piscanec, D. Jiang, K.S. Novoselov, S. Roth, A.K. Geim, Phys. Rev. Lett. 97 (2006) 187401, <http://dx.doi.org/10.1103/PhysRevLett.97.187401>, 4 pp.